Clim Dyn (2007) 28:503–516
DOI 10.1007/s00382-006-0200-2

Influence of the oceanic biology on the tropical Pacific climate in a coupled general circulation model

Matthieu Lengaigne · Christophe Menkes · Olivier Aumont · Thomas Gorgues · Laurent Bopp · Jean-Michel André · Gurvan Madec

Received: 27 April 2006 / Accepted: 25 September 2006 / Published online: 3 November 2006

Abstract The influence of chlorophyll spatial patterns and variability on the tropical Pacific climate is investigated by using a fully coupled general circulation model (HadOPA) coupled to a state-of-the-art biogeochemical model (PISCES). The simulated chlorophyll concentrations can feedback onto the ocean by modifying the vertical distribution of radiant heating. This fully interactive biological-ocean-atmosphere experiment is compared to a reference experiment that uses a constant chlorophyll concentration (0.06 mg m^{-3}). It is shown that introducing an interactive biology acts to warm the surface eastern equatorial Pacific by about 0.5°C. Two competing processes are involved in generating this warming: (a) a direct 1-D biological warming process in the top layers (0–30 m) resulting from strong chlorophyll concentrations in the upwelling region and enhanced by positive dynamical feedbacks (weaker trade winds, surface currents and upwelling) and (b) a 2-D meridional cooling process which brings cold off-equatorial anomalies from the subsurface into the equatorial mixed layer through the meridional cells. Sensitivity experiments show that the climatological horizontal structure of the chlorophyll field in the upper layers is crucial to maintain the eastern Pacific warming. Concerning the variability, introducing an interactive biology slightly reduces the strength of the seasonal cycle, with stronger SST warming and chlorophyll concentrations during the upwelling season. In addition, ENSO amplitude is slightly increased. Similar experiments performed with another coupled general circulation model (IPSL-CM4) exhibit the same behaviour as in HadOPA, hence showing the robustness of the results.

M. Lengaigne
Centre for Global Atmospheric Modeling,
University of Reading, Reading, UK

M. Lengaigne (✉) · C. Menkes · O. Aumont ·
T. Gorgues · J.-M. André · G. Madec
Laboratoire d'Oceanographie et de Climatologie:
Experimentations et Analyses Numériques (LOCEAN),
Couloir 45-55, 4ème étage, Case 100, 4 place Jussieu,
75252 Paris Cedex 05, France
e-mail: lengaign@lodyc.jussieu.fr

L. Bopp
Laboratoire des Sciences du Climat et de l'Environnement,
Saclay, France

1 Introduction

Chlorophyll and related pigments are known to strongly absorb light in the blue and red frequencies and can therefore modify the vertical distribution of radiant heating (Lewis et al. 1990; Sathyendranath et al. 1991). The tropical Pacific is a key region to study these biophysical feedbacks as its equatorial upwelling supplies nutrients, giving rise to a chlorophyll maximum at the equator. Moreover, the ocean biology in the tropical Pacific is strongly influenced by seasonal to interannual climate variations, in particular by El Niño/La Nina transitions that are mainly controlled by upwelling processes (decrease productivity during El Nino, increase during La Nina; Barber et al. 1996; Chavez et al. 1999). These spatial variations of chlorophyll in the tropical Pacific and their related temporal variability have been suggested to significantly impact the upper-ocean heat budget by the recent

observational study of Strutton and Chavez (2004), which have estimated the mixed layer biological heating rate in the central-eastern equatorial Pacific to range between 0.1°C month^{-1} for El Niño conditions and 1°C month^{-1} for La Niña conditions.

Given the importance of phytoplankton on upper-ocean heat budget, modelling studies using forced ocean general circulation models (OGCMs; Nakamoto et al. 2001; Murtugudde et al. 2002; Manizza et al. 2005) have tried to assess the effect of ocean biology on the average surface layer temperatures and circulation in the equatorial Pacific. Their results were contradictory showing either a SST warming (Murtugudde et al. 2002) or a SST cooling (Manizza et al. 2005; Nakamoto et al. 2001) of order of 1°C in the eastern equatorial Pacific. Given the potential amplitude of the SST response in the tropical regions, ocean-atmosphere feedbacks are likely to be important. Simple or hybrid coupled ocean-atmosphere models have therefore been used to further explore the influence of ocean biology on the tropical Pacific climate (Timmermann and Jin 2002; Marzeion et al. 2005). In these studies, bio-optical feedbacks are able to change drastically the model climatology and variability. More specifically, Marzeion et al. (2005) suggests that introducing an interactive biological model acts to damp the seasonal cycle in the eastern Pacific which in turn leads to a strong increase in ENSO variability. This study suggests that the positive coupled ocean-atmosphere Bjerknes (1969) feedback that acts to generate and/or reinforce positive SST anomalies through a reduction of the trade winds is crucial to explain the tropical climate response to ocean biology. However, the simplicity of the atmospheric and/or biological models used in these studies raised the question of how these changes hold in the context of more complex ocean-atmosphere coupled general circulation models (CGCMs). The aim of this study is to investigate further the influence of the biological activity on the tropical climate using a full CGCM coupled with a state-of-the-art biological model representing space-and-time varying chlorophyll concentrations.

We therefore used a recently developed CGCM (HadOPA) in which the Hadley Centre atmosphere model (HadAM3) is fully coupled to the IPSL/LODYC ocean model (OPA). This model reproduces the tropical Pacific mean state, its mean seasonal cycle and the El Niño events with reasonable skill (Lengaigne et al. 2004, 2006). The oceanic component of this model is coupled to the PISCES 24 compartments ecosystem model of Aumont and Bopp (2006). The atmospheric, oceanic and biological components of this model are briefly described in Sect. 2. Then, the influence of the bio-optical feedbacks on the mean state of the tropical Pacific is investigated in Sect. 3. Section 4 focuses on the modification of seasonal and interannual variability induced by those feedbacks. Finally, discussion and concluding remarks are given in Sect. 5.

2 The model

2.1 Ocean/atmosphere coupled model

The ocean-atmosphere coupled GCM used for this study combines the OPA ocean model with the HadAM3 atmospheric model and is called HadOPA (see documentation at http://www.met.rdg.ac.uk/~ericg/hadopa_project.html). A brief description of these models and the coupling procedure is given below.

The atmospheric component of HadOPA is the atmospheric version of the UK Met Office Unified Model (UM), HadAM3. The model has a horizontal resolution of 3.75° longitude × 2.5° latitude, with 19 levels in the vertical, corresponding to a layer thickness of about 100 hPa in the mid-troposphere but with higher resolution in the boundary layer and around the tropopause. Convection is parameterized using the mass-flux scheme of Gregory and Rowntree (1990) with the addition of convective momentum transport (Gregory et al. 1997). A more detailed description of this model and its performance in Atmospheric Model Intercomparison Project (AMIP)-type integrations can be found in Pope et al. (2000) and references therein. The quality of the AGCM simulation of ENSO has been studied extensively by Spencer and Slingo (2003) who showed that in the tropics, the UM reasonably captures the associated precipitation and large-scale circulation anomalies.

The oceanic component of HadOPA is the OPA OGCM in its global configuration, known as ORCA2 (Madec et al. 1998, see also documentation at http://www.lodyc.jussieu.fr/opa/). The model uses a tripolar grid with 2° zonal resolution, and a meridional resolution varying from 0.5° at the equator to 2°cosϕ poleward of 20°. The grid features two points of convergence in the Northern Hemisphere, both situated on the continent. The model has 31 vertical levels with a spacing of 10 m in the upper 150 m, increasing to 500 m in the deep ocean. The model uses a free surface formulation (Roullet and Madec 2000). Vertical eddy viscosity and diffusivity coefficients are computed from a turbulent closure scheme based on a prognostic equation for the turbulent kinetic energy (Blanke and Delecluse 1993), allowing an explicit formulation of

the mixed layer as well as minimum diffusion in the thermocline. Lateral mixing is of Laplacian type and acts along isopycnals (Lengaigne et al. 2003). There is no interactive sea-ice model in this configuration: sea-ice cover is relaxed towards observed monthly climatology. This OGCM has been extensively validated in uncoupled mode in the tropics where it closely matches the observations (e.g. Stoens et al. 1999; Vialard et al. 2001; Lengaigne et al. 2003).

In this OGCM configuration, a particular attention has been paid to the parameterisation of the solar heat flux radiation as it strongly retroacts with the biological model. The ocean heat flux solar radiation Q_{sr} consists of energy distributed across a wide spectral range. The ocean is strongly absorbing for wavelengths longer than 700 nm and these wavelengths contribute to heating the upper few centimetres. The fraction of total solar flux that resides in these non-penetrative wavebands R is assumed, as commonly done, to be 58%. For shorter wavelengths (400–700 nm), the ocean is more transparent, and solar energy crossing the air–sea interface propagates to depths where it contributes to a penetrating flux of solar energy and to local heating below the surface. In state-of-the-art OGCM simulations, a monochromatic formulation of the penetrative solar irradiance $I_{pen}(z)$ is usually assumed following a single exponential profile (Paulson and Simpson 1977):

$$I_{pen}(z) = Q_{sr}(1 - R)e^{-z/h_0},$$

where the value h_0 represents the e-folding depth scale for the penetration of irradiance over the penetrative wavebands. In the standard version of the OPA model, h_0 is chosen to be 23 m. This value corresponds to a Type I water in Jerlov's (1968) classification (oligotrophic waters). Thus, the heating rate entering the ocean at level z is $\frac{1}{\rho_0 C_p}\partial_z I_{pen}(z)$ with ρ_0 and Cp, respectively the ocean density and heat capacity.

In that commonly used parameterization, light penetration is supposed to be independent of the visible light wavelength and of the particle load of seawater. Such assumptions have been shown to provide a very crude and simplistic representation of observed light penetration profiles (Morel 1988; Lewis et al. 1990; Morel and Maritorena 2001, see also Fig. 1). Actually, light absorption in the ocean depends on the particle concentration and it is spectrally selective. Morel (1988) has shown that an accurate representation of light penetration can be provided by a 61-waveband model. Unfortunately, such a model is computationally very expensive. Thus, we have constructed a simplified version of this model in which visible light is splitted into three wavebands: blue (400–500 nm), green (500–600 nm) and red (600–700 nm). For each waveband, the chlorophyll-dependent attenuation coefficient is fitted to the coefficients computed from the full spectral model of Morel (1988) [as modified by Morel and Maritorena (2001)] assuming the same power-law expression. As shown in Fig. 1, this model, called RGB (Read–Green–Blue) model, reproduces quite closely the light penetration profiles predicted by the full spectral model, but with much faster computational efficiency, in contrast to the commonly used monochromatic chlorophyll-independent or chlorophyll-dependent models (Paulson and Simpson 1977; Morel 1988). In this study, the RGB model is used to calculate the oceanic heating rate as well as the phytoplankton light limitation.

The atmospheric and oceanic components have been coupled through OASIS 2.4 (Valcke et al. 2000). No artificial flux corrections are applied at the air–sea interface (except in sea-ice covered region). Air–sea fluxes and SST are exchanged every day. The initial

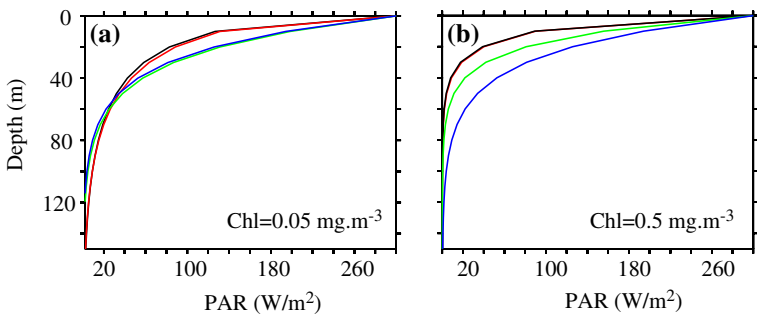

Fig. 1 Penetration profile of the photosynthetically available radiation (*PAR*) calculated by four models. Monochromatic chlorophyll-independent model (OPA standard parameterization; *blue*), monochromatic chlorophyll-dependent model (*green*), 3-waveband RGB model (*red*), 61-waveband Morel (1988) model (*black*) for a vertically homogeneous chlorophyll concentration of **a** Chl = 0.05 mg m^{-3} and **b** Chl = 0.5 mg m^{-3}

conditions of the experiments discussed in this paper are taken to be the last time step of a previous 100-year simulation, therefore preventing any strong initial drift.

The mean state, seasonal and interannual variability of the tropical Pacific for this HadOPA coupled model have been recently investigated in Lengaigne et al. (2004, 2006). The main features are briefly summarized in the following. The observed mean SST and zonal wind stress are simulated realistically, except for a warm bias in the southeastern tropical Pacific. This model is also shown to fairly well reproduce the tropical variability in the Pacific Ocean. In particular, the seasonal cycle of the equatorial SST is well captured by the CGCM but the model tends to produce a stronger and too regular 3-year ENSO mode compared to observations. Despite this bias, the model simulates the seasonal phase locking of the interannual SST variability with most of the modelled El Niño events having a peak during winter in agreement with observations (Lengaigne et al. 2006) and their temporal evolution has been shown to closely match the observed events (Lengaigne et al. 2004).

2.2 Biological model

To calculate the chlorophyll concentrations that are used to compute the heating rate at each grid point, the ocean model is coupled to a biogeochemical model, the Pelagic Interaction Scheme for Carbon and Ecosystem Studies (PISCES) (Aumont and Bopp 2006). This model is derived from the Hamburg Model of Carbon Cycle version 5 (HAMOCC5) (Aumont et al. 2003). As a detailed description of the model parameterizations can be found on a website (see http://www.lodyc.jussieu.fr/~aumont), the model will be here only briefly presented. It has been designed to suit a wide range of temporal and spatial scales, including quasi-steady state simulations on the global scale. The model has 24 compartments (Fig. 2). It simulates the marine biological activity and describes the biogeochemical cycles of carbon and of the main nutrients (N, P, Si and Fe) which limit phytoplankton growth. Four living pools are represented: two phytoplankton size-classes/groups corresponding to nanophytoplankton and diatoms and two zooplankton size-classes which are microzooplankton and mesozooplankton. There are three non-living compartments: semi-labile dissolved organic matter, small and big sinking particles. All the non-living compartments experience aggregation due to turbulence and differential settling. Nutrients are supplied to the ocean from three different sources: atmospheric dust deposition, rivers and sediment mobilization. Iron deposition from the atmosphere has been estimated from the climatological monthly maps of dust deposition simulated by the model of Tegen and Fung (1995) assuming constant values for the iron content and solubility (Moore et al. 2004). River discharge of carbon is taken from the Global Erosion Model of Ludwig et al. (1996). Fe, N, P and Si supplies are derived from the model output by considering globally constant Fe/P/N/Si/C ratios in the rivers. Reductive mobilization of iron from marine sediments has been recognized as a significant source to the ocean. Unfortunately, almost no quantitative information is available to describe this potentially important source. In a way similar to Moore et al. (2004), we have crudely parameterized this input of iron. The initial values of the PISCES model are taken from forced simulations of Aumont and Bopp (2006) where further information about the model equations and parameters can be found.

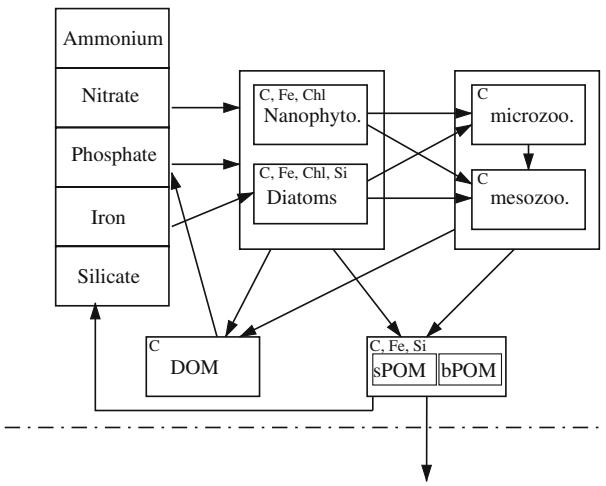

Fig. 2 Schematic of the biogeochemical PISCES model (Aumont and Bopp 2006)

3 Influence of the biological activity on the tropical Pacific mean climate

3.1 The fully coupled experiment

This first 100-year coupled experiment simulates the full biological-ocean-atmosphere interactions (ChlFULL). The chlorophyll concentration produced by the biological component retroacts on the penetrative irradiance via the RGB model. The modelled chlorophyll patterns of ChlFULL (Fig. 3a) are first compared to a mean satellite SeaWifs (McClain et al. 1998) chlorophyll field spanning 1998–2004 (Fig. 3b). The coupled model is able to reproduce the major chloro-

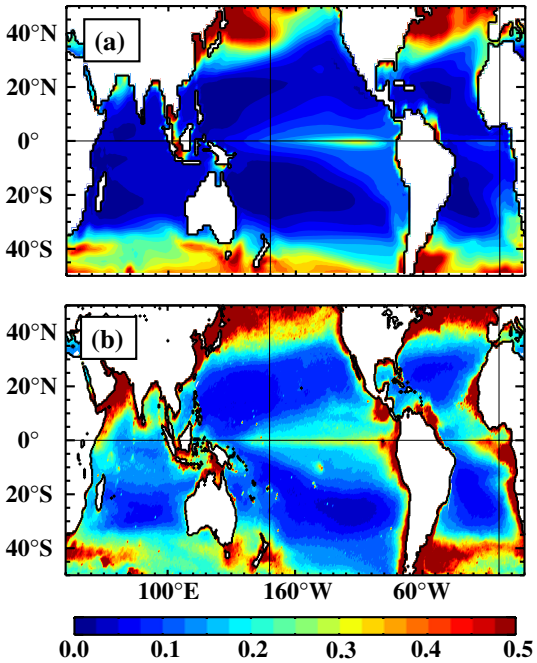

Fig. 3 Annual mean fields of chlorophyll concentrations from **a** observed satellite SeaWiFs data (McClain et al. 1998) from 1999 to 2004 and **b** ChlFULL coupled experiment in the first 30 m. Units are in mg m^{-3}

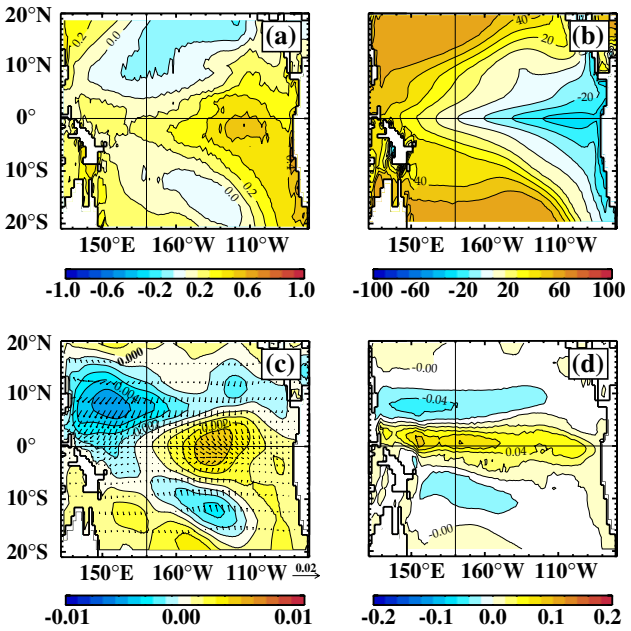

Fig. 4 Annual mean differences between ChlFULL and Chl0.06 experiments in the tropical Pacific for **a** the SST, **b** the euphotic depth, **c** the zonal wind stress (*color*) and wind stress vectors (*arrow*), and **d** the surface zonal current. Contour intervals are 0.1°C for SST, 10 m for the euphotic depth, 0.001 N m^{-2} for zonal wind stress and 0.02 m s^{-1} for current

phyll structures except in the coastal upwelling regions and in the subtropical gyres where it produces too oligotrophic waters. Also, the equatorial Atlantic and Indian Ocean values are largely underestimated. The tropical Pacific ocean is simulated quite realistically with values reaching 0.3 mg m^{-3} in the equatorial upwelling in agreement with the values found in SeaWifs data (Fig. 3b), a reassuring result as the first objective of this study is to understand the bio-optical feedbacks in the tropical Pacific.

To assess the influence of the fully interactive chlorophyll on the tropical Pacific climate, ChlFULL experiment is first compared to another 100-year coupled simulation using a constant chlorophyll concentration of 0.06 mg m^{-3} to calculate the ocean radiant heating (hereafter Chl0.06). This value is representative of the mean ChlFULL chlorophyll averaged in the top 30 m over the (30°N–30°S, 130°E–80°W) region thus representing a ''mean'' surface chlorophyll for the tropical Pacific.

Figure 4a shows that, compared to an ocean with constant chlorophyll concentration (0.06 mg m^{-3}), the main effect of introducing the interactive chlorophyll in the tropics is to globally warm the upwelling and chlorophyll rich region by at most 0.5°C and to slightly cool the most oligotrophic regions. Accordingly, the euphotic depth differences (Fig. 4b) are negative in the upwelling regions due to a stronger heat trapping in the surface layers (the euphotic depth is defined here as the depth where photosynthetically available radiation falls to 1% of its value just below the surface). It is important to stress that the net surface heat flux anomalies (not shown) that respond to SST differences shown in Fig. 4a act to damp these SST differences. Thus, in the following, the changes produced in temperature cannot be driven by the surface flux changes. In addition, the mixed layer depth differences in the equatorial band are very weak (less than 2 m) and therefore do not significantly contribute to the simulated surface warming, in contrast to Murtugudde et al. (2002) and Marzeion et al. (2005) results. As far as wind is concerned, the atmosphere responds to the SST anomalies by creating a trade wind weakening (~10%) and convergence in the central-eastern equatorial Pacific. Additionally, convergence is reduced in the tropical convergence zones (Fig. 4c). The equatorial trade wind weakening acts as a positive retroaction amplifying the positive SST anomalies trough a reduction of the equatorial upwelling in the eastern Pacific (see Fig. 5f). In addition, the amplitude of the South Equatorial Current (SEC) is also weakened by about 10% at the equator (Fig. 4d). This SEC reduction also acts to amplify the SST warming through reduced zonal advection of cold waters from the east.

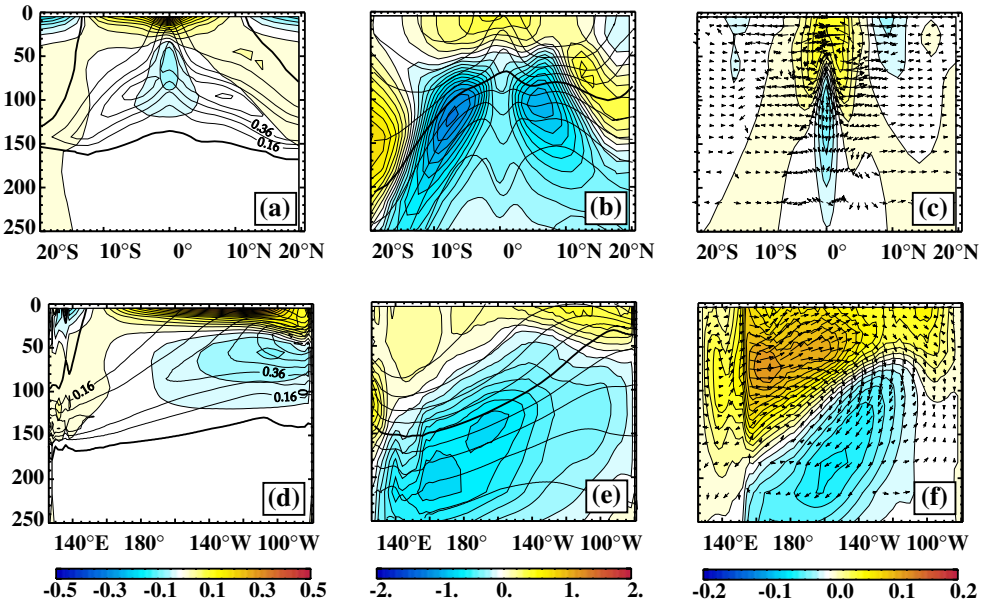

Fig. 5 Meridional sections in the eastern Pacific (20°N–20°S; 130°W–110°W) for **a** ChlFULL chlorophyll concentrations (*contour*) and ChlFULL–Chl0.06 heating rate differences (°C month^{-1}) (*color*), **b** ChlFULL–Chl0.06 temperature anomalies (*color*) and ChlFULL temperature (*contour*), and **c** ChlFULL–Chl0.06 zonal currents (*color*) and meridional currents (*arrows*). **d–f** Same as (**a**)–(**c**) but zonal sections at the equator. Contour intervals are 0.10 mg m^{-3} for chlorophyll concentrations and 2°C for temperatures. The 0.06 mg m^{-3} chlorophyll isoline and 20°C isotherm are thickened

Vertical sections are shown Fig. 5 to further document the ocean response to biology. First, the chlorophyll patterns in the eastern Pacific show a classical structure with subsurface maxima (~0.5 mg m^{-3}) located at the thermocline levels and that deepen off equator as the thermocline spreads (Fig. 5a). The corresponding equatorial zonal section (Fig. 5d) shows an east–west tilt of the surface chlorophyll maximum following the thermocline slope, with increasing chlorophyll values in the upwelling regions. These patterns and values are in qualitative agreement with in situ chlorophyll observations [see Fig. 4 from Marzeion et al. (2005) and the web page http://www.bio-loc.oce.orst.edu/strutton/research_eqpac.htm].

Compared to the constant chlorophyll run (Chl0.06), the spatial structure of chlorophyll in ChlFULL acts to modify the heating rate as follows. As shown in Fig. 5a, chlorophyll concentrations in ChlFULL exceed 0.06 mg m^{-3} approximately between 12°N and 12°S in the eastern Pacific (see thick line in Fig. 5a). Thus, more heat is trapped in the surface layers and consequently, less heat is deposited below. This leads to positive heating rate differences in the first 30 m and negative at depth in that region. This direct bio-induced thermal warming in the surface layers which originates from the direct attenuation of photosynthetically available radiation in the mixed layer leads to a net warming of the upper-eastern equatorial Pacific by about 0.1–0.5 K month^{-1}. This simulated magnitude of the direct bio-induced warming is slightly weaker than the one estimated by the recent observational study of Strutton and Chavez (2004) (about 0.1–1 K month^{-1}). This is mainly due to the reference chlorophyll concentration used to calculate this biological heating rate, 0.06 mg m^{-3} in our study compared to 0 mg m^{-3} in the study of Strutton and Chavez (2004). Off 12°, the opposite process takes place resulting in negative heating rate anomalies in the top 30 m and positive below.

The maximum temperature changes are found in the thermocline core where the vertical gradients are maximum (Fig. 5b). The temperature differences at depth are characterized by two negative off equatorial lobes located around 10° with values reaching ~–1°C surrounding weaker equatorial anomalies at depth. To the south and north of this area, positive subsurface maxima are found. The top 30 meters contrast with the subsurface patterns with positive temperature anomalies between 12°S and 12°N with values reaching 0.4°C at the surface and slightly negative anomalies beyond 12°. At first glance, these differences are consistent with the heating rate anomalies. Moreover, the weaker subsurface equatorial cooling compared to the off-equatorial regions is likely to be the result of the equatorial reduction of the trade wind intensity (Fig. 4c). Indeed, this trade winds weakening acts to reduce the equatorial upwelling (Fig. 5c) by about 5%, a dynamical feedback that counteracts the direct bio-induced thermal cooling in the equatorial thermocline. As shown on the equatorial section in Fig. 5e, the heating rate anomalies are seen to decrease from east to west in response to the chlorophyll east–west gradient. Consistently, temperature surface anomalies decrease from east to west.

As far as zonal currents are concerned, Fig. 5c, f reflects the surface changes (Fig. 4d) with weaker SEC,

North Equatorial Counter Current (NECC) and South Equatorial Counter Current (SECC). At first order, the SEC weakening results from the thermocline shallowing on both sides of the equator implied by the strong off equatorial negative anomalies (Fig. 5c), in agreement with the results of Nakamoto et al. (2001). Indeed, this shallowing reduces the meridional slope of the thermocline on both sides of the equator, which reduces the SEC via geostrophy (not shown). The SEC weakening provokes a shallowing of the EUC, which is reflected by a dipole pattern on Fig. 5e, f. The upper part of the Equatorial Under Current (EUC) is strengthened up to 0.15 m s^{-1} in the western-central Pacific while its lower part is weakened by about 0.06 m s^{-1} in ChlFULL.

3.2 Sensitivity experiments

To investigate the processes at work, sensitivity experiments with prescribed chlorophyll structures are performed. Here, the strategy is to identify the contribution of the temporal, vertical or horizontal variations of the chlorophyll field in generating the SST anomaly displayed in Fig. 4a. To that end, three other 100-year coupled experiments (ChlCST, ChlVERT, Chl0.17) are performed in which either the time or the spatial (horizontal or vertical) variations of the chlorophyll field are kept constant. To that end, ChlCST experiment uses ChlFULL annual mean chlorophyll field to compute the biooptical feedbacks in order to assess the influence of the chlorophyll time variations in generating the SST warming. ChlVERT uses the mean 0–30 m averaged chlorophyll value of ChlCST everywhere on the vertical. This experiment thus displays a horizontal surface chlorophyll structure similar to ChlCST but with no variation on the vertical. Finally, Chl0.17 uses a time-space constant chlorophyll (as in Chl0.06) using the mean ChlFULL chlorophyll value in the equatorial upwelling (2°N–2°S; 180°W–80°E) averaged in the top 30 m (i.e. a value of 0.17 mg m^{-3}). This experiment allows us to investigate how the near surface equatorial values influences the bio optical feedbacks producing the main equatorial patterns seen in Fig. 4.

Figure 6 shows the SST response for these sensitivity experiments. Compared to a full time and depth varying chlorophyll structure (ChlFULL; Fig. 4a), suppressing the time variations (ChlCST; Fig. 6a) and the vertical profile (ChlVERT; Fig. 6b) of the chlorophyll distribution do not modify the overall pattern of SST anomalies with an eastern Pacific equatorial warming for both experiments. Nevertheless, the intensity of this warming is modulated by the chlorophyll structure used to calculate the oceanic heating rate. Whereas in ChlFULL this warming reaches 0.4°C, it is slightly reduced in ChlCST (~0.3°C) and increased in ChlVERT (~0.6°C). In CHLVERT, we chose to integrate the chlorophyll pattern over 30 m. Choosing another integration depth would have changed the intensity of the warming. However, as discussed in Sect. 5, this arbitrary choice neither modifies the sign of the SST anomaly nor its spatial structure. In contrast, imposing a 0.17 constant chlorophyll (Fig. 6c) acts to cool the equatorial region by ~–0.4°C, a pattern opposite to that produced by ChlFULL, CHLCST and CHLVERT simulations. It has to be noticed that using a higher time-space constant chlorophyll concentrations (Chl = 0.34 mg m^{-3}) results in an even stronger equatorial cooling (up to –0.8°C; not shown). These experiments therefore suggest that the horizontal chlorophyll structure is the key factor in generating the eastern equatorial SST warming in ChlFULL.

Vertical sections in the eastern Pacific displayed in Fig. 7 allows us to better understand the differences between Chl0.17 and ChlFULL experiments. This figure illustrates the fact that two main mechanisms are at work to create the equatorial SST anomalies of ChlFULL and Chl0.17. In ChlFULL, as described before (see Sect. 3.1), increased heating rate in the surface layers acts to warm the SST while at depth, decreased

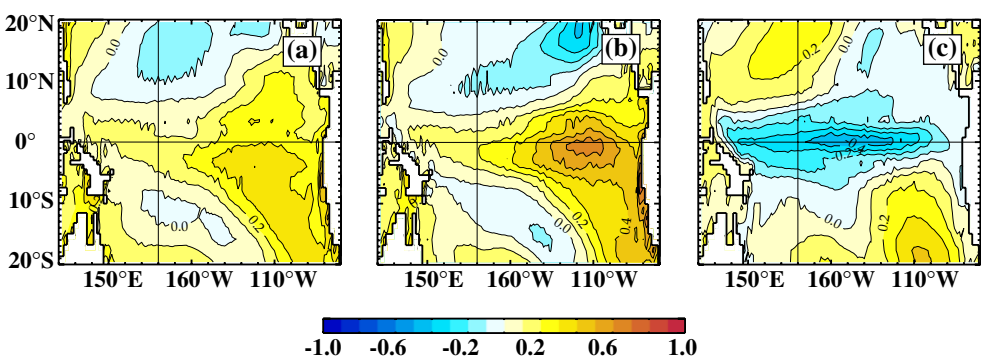

Fig. 6 Annual mean SST differences in the tropical Pacific between **a** ChlCST and Chl0.06, **b** ChlVERT and Chl0.06, and **c** Chl0.17 and Chl0.06. Contour interval is 0.1°C

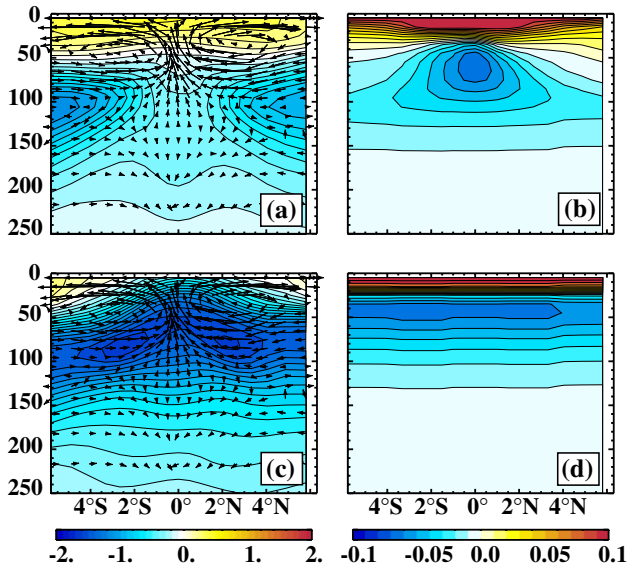

Fig. 7 Meridional sections in the eastern Pacific (6°N–6°S; 130°W–110°W) for **a** temperature differences between ChlFULL and Chl0.06 (*color*) and Chl0.06 currents (*arrows*) and **b** heating rate differences (°C month^{-1}) between ChlFULL and Chl0.06. **c**, **d** Same but for differences between Chl0.17 and Chl0.06

heating rate acts to cool the thermocline (Fig. 7a, b). On top of this 1-D vertical mechanism, a second mechanism acts to bring cold waters in the equatorial zone through the meridional cells (Fig. 7a). These cells advect the off-equatorial cold subsurface anomalies generated off equator near 5° to the equator where they are upwelled. These are the classical meridional circulations associated with the EUC convergence and surface divergence (Fig. 7a). It is of importance to stress that, these two mechanisms compete to produce the modelled SST anomaly patterns.

With these two mechanisms at hand, one can understand the patterns in Chl0.17. The two heating rate patterns (Fig. 7b, d) are similar at the equator but strongly differ off the equator with significantly weaker cooling at depth for ChlFULL. This is related to the chlorophyll patterns difference between ChlFULL and CHL0.17. Whereas ChlFULL chlorophyll concentrations are close to 0.17 mg m^{-3} near the equator, they are significantly lower than this value off 2° (Fig. 5b). Thus, at the equator, through the 1-D vertical mechanism, heating rate anomalies in Chl0.17 will act to warm the surface and cool the subsurface as in ChlFULL. However, the stronger off equatorial cooling in Chl0.17 is advected to the equator through the meridional cells (Fig. 7c) increasing the equatorial cooling and eventually preventing any SST warming.

To conclude on the climatological structures, introducing a fully interactive chlorophyll in a CGCM acts to warm the equatorial cold tongue. First, the strong surface chlorophyll concentrations at the equator act to trap more heat in the top layers (0–30 m) generating an SST warming enhanced by a trade wind reduction and reduced SEC zonal advection. The atmospheric coupling thus acts as a positive feedback. However, these surface processes compete with a meridional cooling subsurface process. Increased heating rates in the top layers lead to decreased heating rates below creating cold subsurface anomalies in the upper thermocline, mainly off the equator where thermocline gradients are stronger. These cold subsurface anomalies are advected to the equator where they reach the surface layers. These negative anomalies are not strong enough to overcome the surface warming processes in ChlFULL experiment.

4 Influence of the biology on the tropical Pacific variability

4.1 Seasonal features

Figure 8a illustrates the seasonal variations of chlorophyll concentrations in ChlFULL. In the eastern equatorial Pacific Ocean, maximum chlorophyll concentrations develop in phase with enhanced trades during July–December, leading to stronger upwelling and enhanced upwelled nutrient in the euphotic layer, as in observations. Accordingly, the positive SST anomaly between ChlFULL and Chl0.06 (Fig. 8b) and its related trade wind relaxation are maximum during

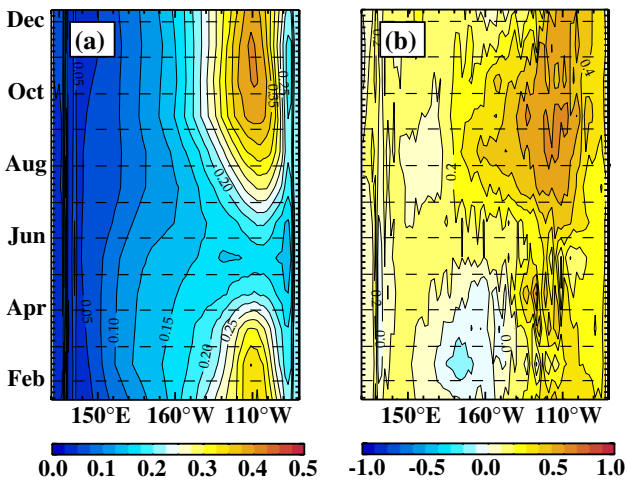

Fig. 8 Time–longitude seasonal cycle in the equatorial Pacific for **a** surface chlorophyll concentrations and **b** SST differences between ChlFULL and Chl0.06. Contour intervals are 0.1°C for temperature and 0.025 mg m^{-3} for chlorophyll concentrations

that time period, as more heat is trapped in the surface layers. However, these SST anomalies decrease significantly from December to March while chlorophyll values remain strong, also suggesting that this SST signal cannot be controlled only by 1-D vertical processes.

These surface equatorial signals are associated to specific vertical structures shown on Fig. 9a, b. The positive temperature anomalies extend down to 100 m in boreal summer during which weak negative temperature anomalies are found at depth (Fig. 9b). These maximum are in phase with strong westward current anomalies in the surface layers which act as a positive dynamical feedback enhancing the surface warming (Fig. 9a). In contrast, the warming shallows and reduces during the following winter and spring as maximum subsurface cold anomalies develop in the upper thermocline (Fig. 9b). In order to explain these variations, the vertical temperature structure off the equator in the meridional recirculation cells at 4°N is shown on Fig. 9c. In that area, cold temperature anomalies reside in the upper thermocline during the whole year while maximum meridional circulation intensifies seasonally during boreal winter and spring. Therefore, it is likely that the meridional cell mechanism evoked in the previous section is at work: the reinforcement of the cells during winter and spring advects the off-equatorial cold temperature anomalies toward the equator explaining the coldest temperature anomalies on Fig. 9b seen at depth. These anomalies act to damp the surface warming leading to the seasonal variations seen on Fig. 8b.

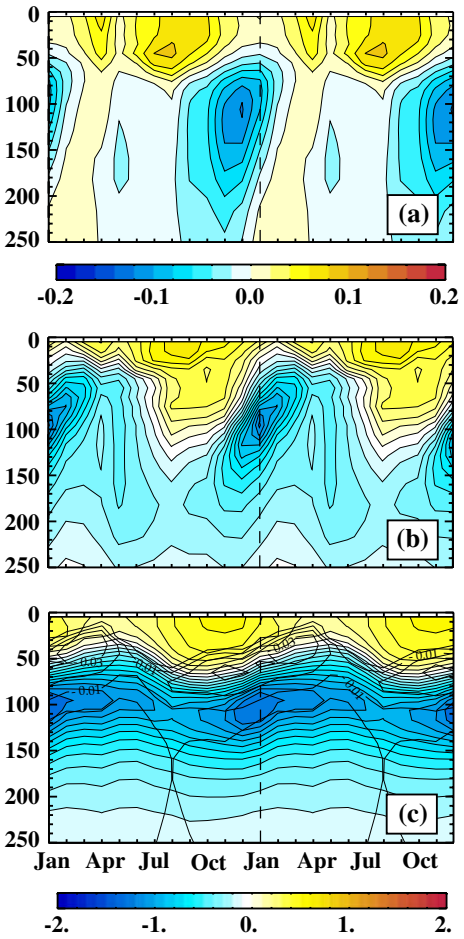

Fig. 9 Time–depth evolution of ChlFULL–Chl0.06 differences in the eastern Pacific (130°W–110°W) for **a** equatorial current, **b** equatorial temperature, and **c** temperature at 4°N. Contours in panel (**c**) shows negative Chl0.06 meridional current at 4°N. Contour intervals is 0.01 m s^{-1} for meridional current (only negative values are shown)

4.2 Interannual features

Thus consistent with the climatological features, it is the association of the 1-D heating mechanism with the 2-D meridional cell cooling mechanism that explains the seasonal variations of the SST anomalies. To briefly tackle the interannual variability, standard deviation and spectra of interannual (defined as the full signal minus seasonal cycle) Niño3 SST anomalies for the ChlFULL and Chl0.06 are computed and presented in Fig. 10. First, introducing fully interactive biology increases the standard deviation by 10%. This result is in agreement with previous studies on ENSO-interannual cycle interactions (e.g. Guilyardi 2006; Fedorov and Philander 2001; Liu 2002) suggesting that the amplitude of El Nino is an inverse function of the strength of the seasonal cycle. The slightly reduced amplitude of the equatorial seasonal cycle with an interactive biology may give ENSO more freedom to develop. This ENSO increase when using an interactive biology has also been suggested by Marzeion et al. (2005) who

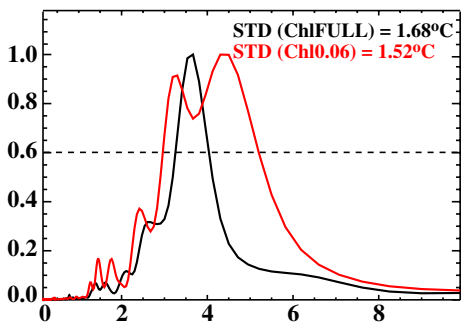

Fig. 10 Normalized power spectra and interannual standard deviation of Niño3 SSTA for Chl0.06 (*red line*) and ChlFULL (*black line*) experiments with HadOPA coupled model. Spectral peaks exceeding 0.6 are significant

examined a hybrid coupled model. Concerning ENSO dominant frequency, while there is a single and clear peak at 3.7 years in the ChlFULL experiment, Chl0.06 spectra is broader with several peaks between 2 and 6 years, and a maximum peak centred at 4.3 years. While the spectra are significantly changed, the evolution of the modelled El Niño and La Niña events is not modified with the introduction of the full biology (not shown). The physical mechanisms responsible for the ENSO spectra changes are however difficult to identify due to the complexity of the coupled model used is this study and therefore the numbers of oceanic and atmospheric changes that could alter the ENSO spectral characteristics.

5 Discussion and conclusion

In this study, we investigated the influence of the bio-optical feedbacks onto the tropical Pacific climate using a CGCM (HadOPA) coupled with a state-of-the-art biological model (PISCES). The model used here shows realistic circulation, thermohaline and chlorophyll patterns in the tropical Pacific region. Several other studies have explored how these feedbacks, in the Pacific, may change the ocean in forced OGCMs (Nakamoto et al. 2001; Murtugudde et al. 2002; Manizza et al. 2005), in intermediate and hybrid coupled models (Timmermann and Jin 2002; Marzeion et al. 2005) and in a CGCM (Wetzel et al. 2006). Nakamoto et al. (2001) and Murtugudde et al. (2002) used a prescribed climatological attenuation depth derived from satellite chlorophyll data, in order to mimic the influence of the biology in the ocean. In the other studies, interactive chlorophyll is used either in the form of simple statistical relationships with temperature (Timmermann and Jin 2002) or with more complex biological models (Marzeion et al. 2005; Manizza et al. 2005; Wetzel et al. 2006).

As far as climatology is concerned, including an interactive biogeochemical model in our CGCM induces a surface warming of the eastern Pacific of about 0.5°C. While forced oceanic experiments display contradictory results in the equatorial Pacific with either positive SST anomalies (Murtugudde et al. 2002), or negative SST anomalies (Nakamoto et al. 2001; Manizza et al. 2005), coupled ocean-atmosphere studies show a consistent SST warming in the eastern Pacific (Timmermann and Jin 2002; Marzeion et al. 2005; Wetzel et al. 2006; this study). Such a consistency between coupled ocean-atmosphere studies may come from the atmospheric retroactions that act to generate and/or reinforce positive SST anomalies. The apparent inconsistency between the forced models results is likely to be related to the way radiation is treated in the control experiments. In fact, Murtugudde et al. (2002) take as a reference an experiment using a constant attenuation depth of 17 m, a depth always lower than the one used in their biological experiment for the tropical Pacific region. They report that including the ocean biology acts to warm the eastern Pacific SST. In contrast, Nakamoto et al. (2001) and Manizza et al. (2005) both used a ''clear water'' assumption in their control experiment with a 23 m attenuation depth (a depth always higher than the one used in their biological experiment) and therefore get an opposite result to Murtuggude et al. (2002), i.e. a cooling of the eastern equatorial Pacific.

The temperature modifications associated with the introduction of a full interactive biology therefore depend on the way radiation is treated in the control experiment. These previous studies usually compared a biological experiment to a control run with a fixed attenuation depth that is either significantly shallower or deeper than the one simulated by the biological model for the tropical Pacific. Most of the related changes discussed in these previous studies are therefore likely to result from the effect of the mean changes of the attenuation depth between both runs and not from the spatial patterns of the chlorophyll distribution in this region. In order to only investigate the latter effect, our fully interactive biological-ocean-atmosphere experiment is compared to a reference experiment that uses a mean reference chlorophyll concentration equal to the mean tropical Pacific chlorophyll concentration modelled by the biological experiment (0.06 mg m^{-3}). It has to be noticed that increasing this reference value increases the amplitude of the surface warming but do not modify its structure or the mechanisms at work. Therefore the discussion will focus on the mechanisms responsible for the changes, but not on the amplitude of the SST changes which depend on the reference used.

We find that the climatological vertical structure of the temperature anomalies are characterized by a warming extending down to ~30 m in the eastern Pacific and a subsurface cooling all along the Pacific in the (10°S–10°N) band. Two main processes are at work to maintain these patterns. First, the existence of strong chlorophyll concentrations in the near-surface equatorial Pacific act to heat the top layers (0–30 m) generating an SST warming enhanced by positive dynamical feedbacks (weakening of the trade winds, the surface currents, and the upwelling). However, these surface processes compete with a cooling subsurface process. Increased heating rates in the top

layers lead to decreased heating rates below creating cold subsurface anomalies in the upper thermocline, mainly off the equator where thermocline gradients are stronger. These cold subsurface anomalies are advected to the equator, by the meridional equatorial cells, where they reach the surface layers. These negative anomalies are not strong enough to overcome the surface warming processes.

Thus the oceanic processes involved in creating the differences induced by the interactive biology combine a direct 1-D biological effect modifying the vertical heating rate and a 2-D meridional advection effect which brings cold off equatorial waters in the equatorial mixed layer. These oceanic mechanisms differ from those previously described in Murtugudde et al. (2002) and Marzeion et al. (2005) where only 1-D processes were invoked such that in Murtugudde et al. (2002), most of the SST anomalies could be reproduced by using a mean attenuation depth for the Pacific without spatial structure. To test if this holds in the CGCM framework, additional experiments were performed.

While the time variations of the chlorophyll field do not significantly change the SST patterns, the horizontal structure of the mean chlorophyll field is crucial to maintain the eastern Pacific warming. Indeed, using a constant chlorophyll concentration higher than the 0.06 mg.m^{-3} value of the reference experiment and closer to the strong eastern equatorial values (e.g. 0.17, 0.34 mg m^{-3}) does not allow the reproduction of the warming and can even cool the ocean surface. In those sensitivity experiments chlorophyll concentrations are systematically stronger than those of the full biology experiment off 2°. This induces stronger off-equatorial subsurface cooling in the thermocline that is advected toward the equatorial mixed layer thus counteracting the 1-D heating mechanism. Hence, in our CGCM framework, use of a spatially variable chlorophyll concentration is needed to reproduce the main action of the biooptical feedbacks. Seasonal variability induced by these feedbacks can also be explained by the combination of these 1-D and 2-D processes. When the meridional cells are strongest in winter and spring, increased subsurface cold waters are advected toward the equator in the mixed layer and SST anomalies are weak. In contrast, in summer and fall, when these cells are reduced, the SST warming is strongest. This seasonal evolution is in agreement with Murtugudde et al. (2002) but contradict Wetzel et al. (2006) study.

Given the diversity of the model responses found in previous studies, we have also tested the sensitivity of our results to the CGCM used. To that end, we performed similar experiments to Chl0.06 and ChlFULL with the IPSL-CM4 model (identical ocean but interactive sea-ice model and LMDz atmospheric model; see Appendix) coupled to the same biological PISCES model. The results obtained with the IPSL-CM4 model are very similar to HadOPA results in terms of mean changes. Figure 11 shows that introducing the biooptical feedbacks act to warm the eastern equatorial Pacific by about 0.5°C, similarly to the HadOPA response (Fig. 4a). In addition, the wind retroaction shows a central Pacific westerly anomaly, acting to generate/amplify the ocean warming as in HadOPA (Fig. 4c). Vertical oceanic changes and mechanisms associated with these biophysical feedbacks are also found to agree with HadOPA results (not shown). This therefore gives us confidence in the robustness of the results presented in this study. However, the influence of the biology on the oceanic temperature results from a subtle balance between a direct 1-D biological warming process in the top layers (0–30 m) and a 2-D meridional cooling process. This balance may therefore be highly model-dependent and result in different temperature patterns with another ocean/biological model.

Finally, we have briefly explored the influence of the interactive biology onto ENSO-like variability in HadOPA and IPSL-CM4 CGCMs. Figures 10 and 12 show the normalized Niño3 SST anomalies spectra of Chl0.06 and ChlFULL experiments in both CGCMs. For both models, introducing an interactive biology alters the energy distribution within the 2–5 year ENSO-band. While in HadOPA the ENSO peak narrows (a degradation compared to observations), the IPSL-CM4 shows the opposite. Reasons for these inconsistent behaviours remain unclear. In contrast, both models show a consistent ENSO amplitude increase of about 10% when introducing the interactive biology. The standard deviation of the Niño3 interannual SST anomalies increases from 1.52 to 1.68°C in

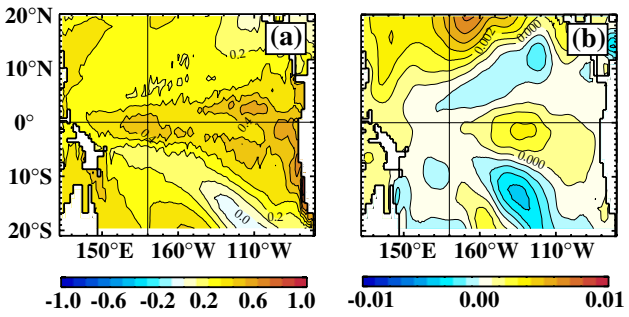

Fig. 11 Annual mean differences between ChlFULL and Chl0.06 experiments with the IPCL-CM4 coupled model in the tropical Pacific for **a** SST, **b** the zonal wind stress. Contour intervals are 0.1°C for SST and 0.001 N m^{-2} for zonal wind stress

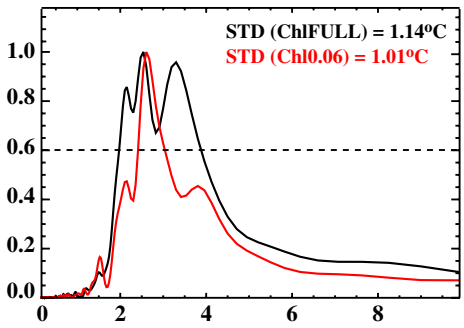

Fig. 12 Normalized power spectra and interannual standard deviation of Niño3 SSTA for Chl0.06 (*red line*) and ChlFULL (*black line*) experiments with IPSL-CM4 coupled model. Spectral peaks exceeding 0.6 are significant

HadOPA and from 1.01 to 1.14°C in IPSL-CM4. Yet, the evolution of the modelled events is not significantly changed (not shown). Marzeion et al. (2005) also reported an amplification of ENSO but with a much stronger increase. In contrast, Timmermann and Jin (2002) and Wetzel et al. (2006) both reported a decrease of ENSO amplitude in their coupled models. These differences may be related to the difference in the way radiation is treated in the control experiments or to the differences in the coupled models used. Contrary to the robustness in the mean state changes, the large variety of ENSO response to biophysical feedbacks and the difficulty to identify the related dominant processes in our coupled models thus makes the assessment of the biology influence on ENSO rather inconclusive.

To conclude, given the classical south-eastern Pacific warm bias and equatorial Pacific cold bias in most coupled models (AchutaRao et al. 2002), the warming induced by the bio-optical feedbacks will reduce the equatorial bias but will further degrade the southeastern Pacific warm bias in these coupled models. Since phytoplankton does interact with light penetration in the real ocean, it is useful to take these interactions into account for further improvement of the CGCM parametrization. Nevertheless, instead of using a fully interactive and costly biological model, this can be accounted for by the use of a constant observed horizontal chlorophyll pattern combined to a spectrally dependent optical scheme such as used here.

Acknowledgments The authors gratefully acknowledge comments of E. Maier-Raimer and an anonymous reviewer that led to significant improvements in an earlier version of the manuscript. They further acknowledge IRD for support, the developers team of the HadOPA and IPSL-CM4 models and the IDRIS centre where computations were carried out. ML also likes to thank J. Slingo, A. Timmermann and F.-F. Jin for invaluable discussion on this work. ML was founded by the Marie Curie Intra-European fellowship MEIF-CT-2003-501143.

6 Appendix: Description of the IPSL-CM4 coupled general circulation model

The IPSL-CM4 model presently couples four components of the Earth system. LMDZ is the component for atmospheric dynamics and physics. OPA-ORCA2 is the component for ocean dynamics (same as in HadOPA and already described in Sect. 2.1). ORCHIDEE handles the land surface and LIM is the component for sea-ice dynamics and thermodynamics.

The atmospheric component of IPSL-CM4 is LMDZ-4 and has been developed at the Laboratoire de Meteorologie Dynamique (LMD). The model has a horizontal resolution of 3.75°longitude × 2.5°latitude, with 19 levels in the vertical. The dynamical part of the code is based on a finite-difference formulation of the primitive equations. In this model, the cloud cover and in-cloud water are deduced from the large scale total water and moisture at saturation, using a Probability Distribution Function (PDF) for the subgrid-scale total water, following Bony and Emmanuel (2001). The PDF moments are diagnosed interactively from the condensated water predicted by the convection scheme at the subgrid scale and from the large-scale degree of saturation of the atmosphere. Condensation is parameterized separately for convective and non-convective clouds. Moist convection is treated using a modified version of the Emanuel (1991) scheme (Grandpeix et al. 2004). A more detailed description of this atmospheric model and its climate performance can be found in Hourdin et al. (2005). This model is coupled to a land surface model (ORCHIDEE) described in Krinner et al. (2005).

The ocean component in this IPSL-CM4 CGCM is the OPA model (Madec et al. 1998, see documentation at http://www.lodyc.jussieu.fr/opa/) in its ORCA2 configuration. This model has already been described in Sect. 2.1. Contrary to HadOPA model, an interactive sea-ice model (LIM) with explicit thermodynamics and prognostically computed sea-ice cover is included in the IPSL-CM4 model. A detailed description of this sea-ice model in Fichefet and Morales Maqueda (1999).

These components have been coupled through OASIS 3 (Valcke et al. 2004). Air–sea, air–ice fluxes and SST are exchanged every day. Ocean–sea-ice are coupled every oceanic time step. Atmosphere and land surface are coupled every atmospheric time step. A full

documentation of this coupled model can be found on http://dods.ipsl.jussieu.fr/omamce/IPSLCM4/Doc-IPSLCM4/FILES/DocIPSLCM4.pdf

References

AchutaRao K, Sperber KR, in collaboration with the CMIP modelling groups (2002) Simulation of the El Niño southern oscillation: results from the coupled model intercomparison project. Climate Dyn 19:191–209

Aumont O, Bopp L (2006) Globalizing ocean in-situ iron fertilization experiments. Global Biogeochem Cycles 20:GB2017. DOI 10.1029/2005GB002591

Aumont O, Maier-Reimer E, Blain S, Monfray P (2003) An ecosystem model of the global ocean including Fe, Si, P colimitations. Global Biogeochem Cycles 17:1060. DOI 10.1029/2001GB001745

Barber RT, Sanderson MP, Lindley ST, Chai F, Newton J, Trees CC, Foley DG, Chavez FP (1996) Primary productivity and its regulation in the equatorial Pacific during and following the 1991–1992 El Niño. Deep Sea Res 43B:933–969

Bjerknes J (1969) Atmospheric teleconnections from the equatorial Pacific. Mon Wea Rev 97:163–172

Blanke B. Delecluse P (1993) Variability of the tropical Atlantic ocean simulated by a general circulation model with two different mixed layer physics. J Phys Oceanogr 23:1363–1388

Bony S, Emmanuel KA (2001) A parameterization of the cloudiness associated with cumulus convection, evaluation using TOGA COARE data. J Atmos Sci 58:3158–3183

Chavez FP, Strutton PG, Friedrich GE, Feely RA, Feldman GC, Foley DG, McPhaden MJ (1999) Biological and chemical response of the equatorial Pacific ocean to the 1997–98 El Niño. Science 286:2126–2131

Emanuel KA, (1991) A scheme for representing cumulus convection in large-scale models. J Atmos Sci 48:2313–2335

Fedorov AV, Philander SG (2001) A stability analysis of tropical ocean–atmosphere interactions: bridging measurements and theory for El Niño. J Clim 14:3086–3101

Fichefet T, Morales Maqueda MA (1999) Modelling the influence of snow accumulation and snow-ice formation on the seasonal cycle of the Antarctic sea-ice cover. Clim Dyn 15:251–268

Grandpeix JY, Phillips V, Tailleux R (2004) Improved mixing representation in Emanuel's convection scheme. Q J R Meteorol Soc 604:3207–3222

Gregory D, Rowntree PR (1990) A mass flux convection scheme with the representation of cloud ensemble characteristics and stability dependent closure. Mon Wea Rev 118:1483–1506

Gregory D, Kershaw R, Inness PM (1997) Parametrisation of momentum transport by convection. II: Tests in single column and general circulation models. Q J Roy Meteor Soc 123:1153–1183

Guilyardi E (2006) El Niño–mean state–seasonal cycle interactions in a multi-model ensemble. Climate Dyn 26:329–348. DOI 10.1007/s00382-005-0084-6

Hourdin F, Musat I, Bony S, Braconnot P, Codron F, Dufresne JL, Fairhead L, Filiberti MA, Friedlingstein P, Grandpeix JY, Krinner G, LeVan P, Li ZX, Lott F (2005) The LMDZ4 general circulation model: climate performance and sensitivity to parametrized physics with emphasis on tropical convection. Climate Dyn DOI 10.1007/s00382-006-0158-0

Jerlov NG (1968) Optical oceanography. Elsevier, London

Krinner G, Viovy N, de Noblet-Ducoudré N, Ogée J, Polcher J, Friedlingstein P, Ciais P, Sitch S, Prentice IC (2005) A dynamic global vegetation model for studies of the coupled atmosphere-biosphere system. Global Biogeochem Cycles 19. DOI 10.1029/2003GB002199

Lengaigne M, Madec G, Menkes C, Alory G (2003) The Impact of Isopycnal mixing on the tropical ocean circulation. J Geophys Res 108. DOI 10.1029/2002JC001704

Lengaigne M, Guilyardi E, Boulanger JP, Menkes C, Delecluse P, Inness P, Cole J, Slingo J (2004) Triggering of El Niño by Westerly wind events in a coupled general circulation model. Climate Dyn 23:601–620. DOI 10.1007/s00382-004-0457-2

Lengaigne M, Boulanger JP, Menkes C, Spencer H (2006) Influence of the seasonal cycle on the termination of El Nino events in a coupled general circulation model. J Clim 19:1850–1868. DOI 10.1175/JCLI3706.1

Lewis MR, Carr ME, Feldman GC, Esias W, McClain C (1990) Influence of penetrating solar radiation on the heat budget of the Equatorial Pacific. Nature 347:543–546

Liu Z (2002) A simple model study of the forced response of ENSO to an external periodic forcing. J Clim 15:1088–1098

Ludwig W, Probst JL, Kempe S (1996) Predicting the oceanic input of organic carbon by continental erosion. Global Biogeochem Cycles 10:23–41

Madec G, Delecluse P, Imbard M, Lévy C (1998) OPA 8.1 Ocean General Circulation Model reference manual. Note du Pôle de modélisation, Institut Pierre-Simon Laplace, No. 11, 91pp

Manizza M, Le Quere C, Watson AJ, Buitenhuis ET (2005) Bio-optical feedbacks among phytoplankton, upper ocean physics and sea-ice in a global model. Geophys Res Lett 32. DOI 10.1029/2004GL020778

Marzeion B, Timmermann A, Murtuggude R, Jin FF (2005) Biophysical feedbacks in the Tropical Pacific. J Clim 18:58–70

McClain CR, Cleave ML, Feldman GC, Gregg WW, Hooker SB, Kuring N (1998) Science quality SeaWiFS data for global biosphere research. Sea Technol 39:10–16

Murtugudde RJ Beauchamp, Busalacchi A (2002) Effects of penetrative radiation in the upper ocean tropical ocean circulation. J Clim 15:470–486

Moore JK, Doney SC, Lindsay K (2004) Upper ocean ecosystem dynamics and iron cycling in a global three-dimensional model. Global Biogeochem Cycles 18:GB4028. DOI 10.1029/2004GB002220

Morel A (1988) Optical modeling of the upper ocean in relation to its biogenous matter content (Case I waters). J Geophys Res 93:10749–10768

Morel A, Maritorena S (2001) Bio-optical properties of oceanic waters: a reappraisal. J Geophys Res 106:7163–7180

Nakamoto S, Prasanna Kumar S, Oberhuber J, Ishizaka J., Muneyama K, Frouin R (2001) Response of the equatorial Pacific to chlorophyll pigment in a mixed-layer isopycnal ocean general circulation model. Geophys Res Lett 28:2021–2024

Paulson CA, Simpson JJ (1977) Irradiance measurements in the upper ocean. J Phys Oceanogr 7:952–956

Pope VD, Gallani ML, Rowntree PR, Stratton RA (2000) The impact of new physical parametrisations in the Hadley Centre climate model-HadAM3. Climate Dyn 16:123–146

Roullet G, Madec G (2000) Salt conservation, free surface and varying volume: a new formulation for Ocean GCMs. J Geophys Res 105:23927–23942

Sathyendranath S, Platt T, Horne EPW, Harrison WG, Ulloa O, Outerbridge R, Hoepffner N (1991) Estimation of new production in the ocean by compound remote sensing. Nature 353:129–133

Spencer H, Slingo JM (2003) The simulation of peak and delayed ENSO teleconnections. J Clim 16:1757–1774

Stoens A, Menkes C, Radenac MH, Dandonneau Y, Grima N, Eldin G, Memery L, Navarette C, Andre JM, Moutin T, Raimbault P (1999) The coupled physical-new production system in the equatorial Pacific during the 1992–1995 El NIno. J Geophys Res 104:3323–3329

Strutton PG, Chavez FP (2004) Radiant heating in the equatorial Pacific: observed variability and potential for real-time calculation. J Clim 17:1097–1109

Tegen I, Fung I (1995) Contribution to the atmospheric mineral aerosol load from land surface modification. J Geophys Res100:18707–18726

Timmermann A, Jin FF (2002) Phytoplankton influences on tropical climate. Geophys Res Lett 29. DOI 10.1029/2002GL015434

Vialard J, Menkes C, Boulanger JP, Delecluse P, Guilyardi E, McPhaden MJ, Madec G (2001) Oceanic mechanisms driving the SST during the 1997–1998 El Niño. J Phys Oceanogr 31:1649–1675

Valcke S, Terray L, Piacentini A (2000) The OASIS coupler user guide version 2.4, Technical report TR/CMGC/00-10, available at Cerfacs, Toulouse, France

Valcke S, Caubel A, Vogelsang R, Declat D (2004) OASIS3 ocean atmosphere sea ice soil user's guide technical report TR/CMGC/04/68, CERFACS, Toulouse, France

Wetzel P, Maier-Reimer E, Botzet M, Jungclaus J, Keenlyside N, Latif M (2006) Effects of ocean biology on the penetrative radiation in a coupled climate model. J Clim 19:3973–3987